*Electronic Supplementary Information*

# Ni@C nanowires enabled photothermal membrane for highly efficient solar-driven interfacial water purification

Cailin Yang, Limingming Huang, Kai Han*

State Key Laboratory for Powder Metallurgy, College of Chemistry and Chemical Engineering, Central South University, Changsha, Hunan 410083, P. R. China.

* Corresponding author, kaihan@csu.edu.cn.

## 1. Experimental Section

**Preparation of precursors of Nickel-based nanowires**

All chemicals were used as purchased without further treatment. The precursors of Nickel-based nanowires were obtained by the one-step hydrothermal method. Specifically, 0.60 g of nitrilotriacetic acid (97%, Shanghai Aladdin Bio-Chem Technology Co., LTD) and 1.49 g of Nickel chloride hexahydrate (AR, 98%, Shanghai Aladdin Bio-Chem Technology Co., LTD) were dissolved in 52.5 mL deionized water and 7.5 mL isopropyl alcohol (AR, Shanghai Aladdin Bio-Chem Technology Co., LTD) under constant stirring, and then the mixture was transferred into a 100 mL Teflon lined stainless steel autoclave and heated at 180 °C for 24 h. After that, the reaction solution was cooled down to room temperature naturally. The obtained product was cleaned with deionized water and ethanol three times and then filtered, and the precursors of Nickel-based nanowires were dried in the oven at 60°C.

**Preparation of Ni@Cnw**

The precursors were laid in a porcelain boat and sent to a tube furnace for heat treatment. Argon gas was introduced into the tubular furnace for 30 min while argon gas velocity was 100 $mL \cdot min^{-1}$ for the whole heat treatment. The temperature was raised at room temperature to 600°C at a rate of 5 $°C \cdot min^{-1}$. After holding for 2 h at 600°C, the tube furnace was cooled down to room temperature naturally, and the black nickel-carbon nanowire powder was recorded as Ni@Cnw.

**Preparation of NiOnw**

The precursors were laid in a porcelain boat and sent to a muffle furnace for heat treatment. The temperature was raised at room temperature to 600°C at a rate of 5 $°C \cdot min^{-1}$. After holding for 2 h at 600°C, the muffle furnace was cooled down to room temperature naturally, and the green nickel oxide nanowire powder was recorded as NiOnw.

**Preparation of Ninw**

The NiOnw were laid in a porcelain boat and sent to a tube furnace for heat treatment.

Hydrogen argon mixture gas was introduced into the tubular furnace for 30 min while hydrogen argon mixture gas velocity was 100 mL·min$^{-1}$ for the whole heat treatment. The temperature was raised at room temperature to 600°C at a rate of 5 °C·min$^{-1}$. After holding for 2 h at 600°C, the tube furnace was cooled down to room temperature naturally, and the nickel nanowire powder was recorded as Ninw.

**Preparation of photothermal conversion membrane**

50 mg of nickel-based nanowire powder was dispersed in a solution of 50 mL of N-methylpyrrolidone (NMP, AR, Shanghai Aladdin Bio-Chem Technology Co., LTD) and 5 g polyvinylidene fluoride (PVDF, HSV900, Shanghai Titan Scientific Co., Ltd.) as a binder, under constant ultrasonication, resulting in a uniform dispersion. Glass fiber filter paper (GF/F, CAT No.1825-047, Whatman International LTD) was used as the membrane substrate. The nanowires were deposited on the surface of the glass fiber filter paper by vacuum filtration. The deposition area was determined based on the diameter of the filter cup, and the amount of dispersion required was calculated according to the desired surface load. A specific amount of the dispersion was transferred to a clean beaker using a pipette, followed by the addition of a large amount of ethanol (AR, Xilong Science & Technology Co., Ltd) to ensure complete dispersion. This mixture was then poured into the vacuum filter to ensure uniform deposition. After drying at 60°C for 24 hours in an oven, a 30 mm diameter cutter was used to cut the nickel-based nanowire photothermal conversion membrane into a fixed size with uniform deposition.

**Preparation of superhydrophobic Ni@Cnw membrane**

100 mg of polydimethylsiloxane (PDMS, AR, DOWSIL™) was added to a beaker, along with 50 mL of n-hexane (AR, Shanghai Aladdin Bio-Chem Technology Co., LTD) as the solvent. Ultrasonic dispersion was employed to dissolve the PDMS in n-hexane fully. The PDMS solution was then sprayed onto the top surface of the Ni@Cnw photothermal conversion membrane obtained in the previous step. After spraying, the membrane was dried in an oven at 60°C to obtain the superhydrophobic Ni@Cnw membrane.

## 2. Materials characterization

The morphology of nickel-based nanowires was photographed by scanning electron microscopy (SEM) and transmission electron microscope (TEM). Energy dispersive spectroscopy (EDS) was used to characterize the element distribution of nickel-based nanowires. X-ray diffraction (XRD) was used to analyze the physical phase of different nickel-based nanowires. The different element composition of each nickel-based nanowire was analyzed by x-ray photoelectron spectroscopy (XPS).

The nickel content in the powder samples was determined using an inductively coupled plasma emission spectrometer (ICP) and thermogravimetric analysis (TGA). TGA is an analytical technique that monitors changes in a material's physical or chemical properties as a function of temperature or time, providing information about various thermal phenomena. Before testing, the powder samples were stored in a drying oven to prevent moisture absorption. An appropriate amount of the powder sample was weighed and placed in an alumina crucible. The heating rate was set to 5°C·min$^{-1}$, with a temperature range from room temperature to 500°C. The gas used during the test was oxygen. The mass fraction data from the TGA was analyzed to determine the nickel content in the sample. Before the ICP test, the powder samples were fully dissolved and

then diluted to a known volume. By analyzing the test data obtained from the ICP, the mass fraction of nickel in the powder samples was calculated. Additionally, ICP was used to characterize the metal ion removal rate of interfacial evaporation.

The imaginary part of the dielectric function of the material was measured using a Vector network analyzer (VNA). Samples with different weight percentages of the Ni@C nanowires, specifically 20 wt% and 40 wt%, were prepared. The measurements were conducted over a frequency range from 2 GHz to 18 GHz. Each sample was tested more than three times, and the average value of these measurements was taken as the final value for the imaginary part of the dielectric function.

The diffuse reflectance of the samples was measured using an ultraviolet/visible/near infrared spectrophotometer in integrating sphere mode. The spectral range for the measurements was 200 nm to 2500 nm. Prior to testing, the membrane samples were wetted using the same method employed during the interface evaporation performance tests. The samples were placed on absorbent cotton swabs and allowed to naturally absorb water until the surface was fully wetted. The scanning speed for the measurements was set to 100 $nm \cdot min^{-1}$.

The thermal conductivity was measured using a thermal conductivity meter. Each sample's thermal conductivity was measured at least three times, and the average value of these measurements was taken as the final thermal conductivity.

The contact angle of water on the photothermal conversion membrane was measured using an Abbe refractometer. The direct measurement method was employed, where the shape of the liquid droplet was captured through photography or videography. The contour of the droplet was approximated by fitting a tangent line at the three-phase contact point using the symmetry axis drawing method. From this contour, the contact angle (θ) was calculated.

## 3. Interfacial evaporation measurements

All experiments in this study were conducted at a temperature of 25±0.5°C and a humidity of 50%±5%. As shown in Figure S6, a xenon lamp was used to simulate sunlight during the interfacial evaporation process. Before each test, the light intensity of the xenon lamp was measured with a solar meter to ensure consistency at the interface height, maintaining a constant intensity of 1 $kW \cdot m^{-2}$.

An electronic balance was used to automatically record the mass change of the device every second, with the data being logged into a computer. The surface temperature of the evaporating membrane and the temperature of the water below were monitored by a thermocouple, while a hygrometer tracked temperature and humidity changes throughout the entire testing process.

The photothermal conversion efficiency ($\eta$) of the samples was calculated using the following formula:

$$\eta = \frac{\dot{m} h_{fg}}{q_{solar}}$$

where $\dot{m}$ is the net evaporation rate, defined as the evaporation rate under illumination ($\dot{m}_{light}$) minus the evaporation rate under dark conditions ($\dot{m}_{dark}$), with units of $kg \cdot m^{-2} \cdot h^{-1}$; $h_{fg}$ is the enthalpy of evaporation of water from room temperature liquid to vapor, including the sensible heat required to raise the temperature of water from room temperature to the evaporation temperature, and the latent heat required for the phase change from liquid to vapor at the

evaporation temperature, with units of kJ·kg$^{-1}$; $q_{solar}$ is the intensity of solar energy, with units of kW·m$^{-2}$.

The equivalent enthalpy of evaporation of water at 25°C and atmospheric pressure was calculated using the following formula:

$$U_{in} = E_0 m_0 = E_{equ} m_g$$

where $E_0$ is the enthalpy of evaporation for conventional water at 25°C (2450 kJ·kg$^{-1}$); $m_0$ is the mass change of the conventional water (units of kg·m$^{-2}$·h$^{-1}$); $E_{equ}$ is the equivalent enthalpy of evaporation for the interface evaporation system (units of kJ·kg$^{-1}$); $m_g$ is the mass change of the interfacial evaporation system (units of kg·m$^{-2}$·h$^{-1}$). This calculation allows us to determine the impact of the interface evaporation system on the enthalpy of evaporation of water (Figure S8), which is essential for subsequent calculations of the solar interface evaporation energy utilization efficiency.

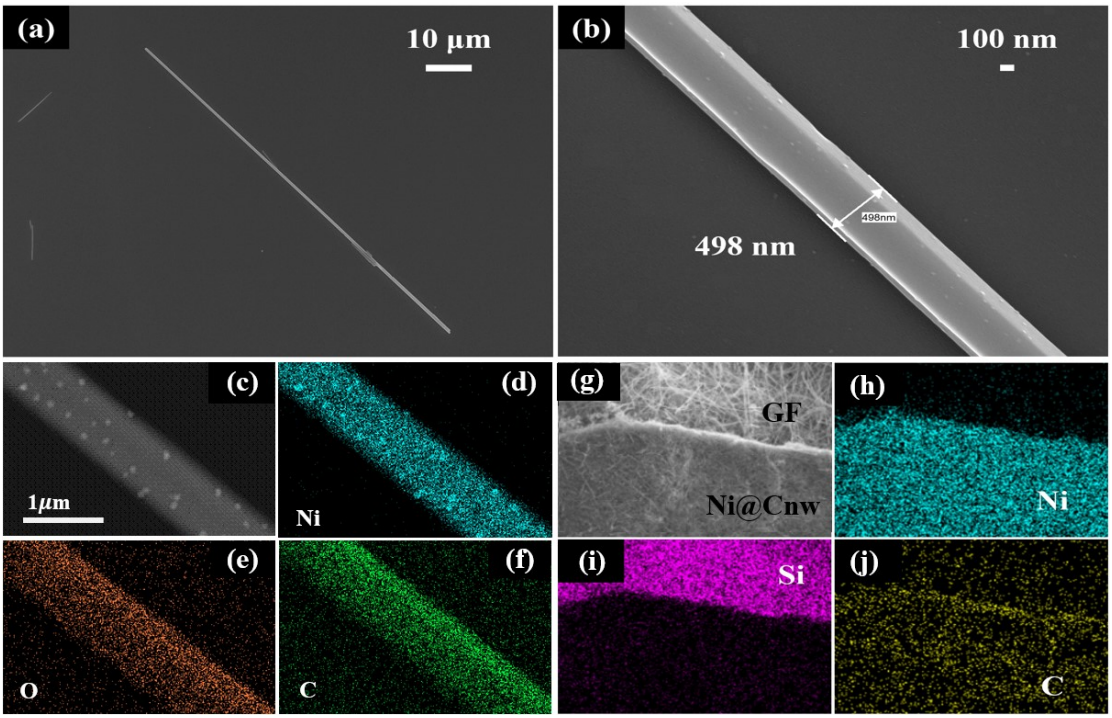


**Figure S1**. SEM diagram. (a) Ni@C nanowires; (b) It is approximately 500 nm in diameter; (c) Pure nickel particles uniformly distributed on the Ni@C nanowire; EDS characterizing element distribution map: (d) Ni; (e) O; (f) C; (g) Ni@C nanowire photothermal conversion membrane; EDS characterizing element distribution map: (h) Ni; (i) Si; (j) C

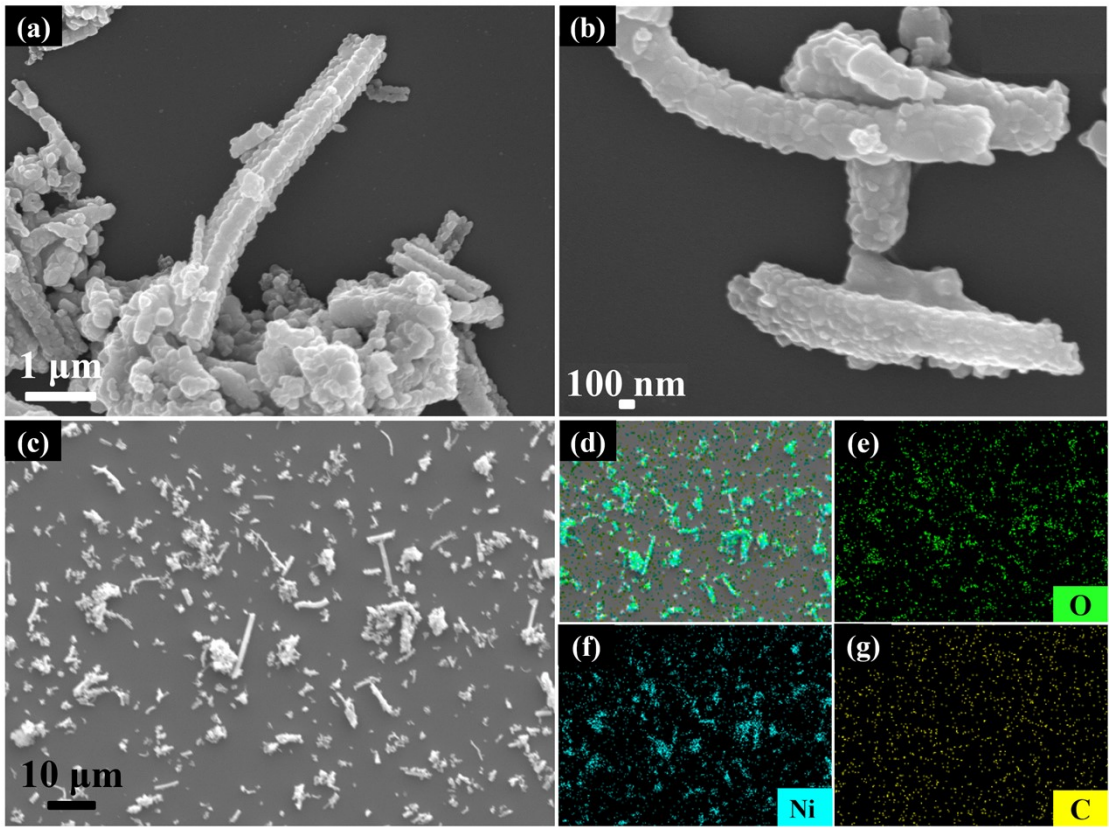


**Figure S2**. SEM image; (a-c) NiOnw; (d-g) EDS characterization, (e) O; (f) Ni; (g) C.

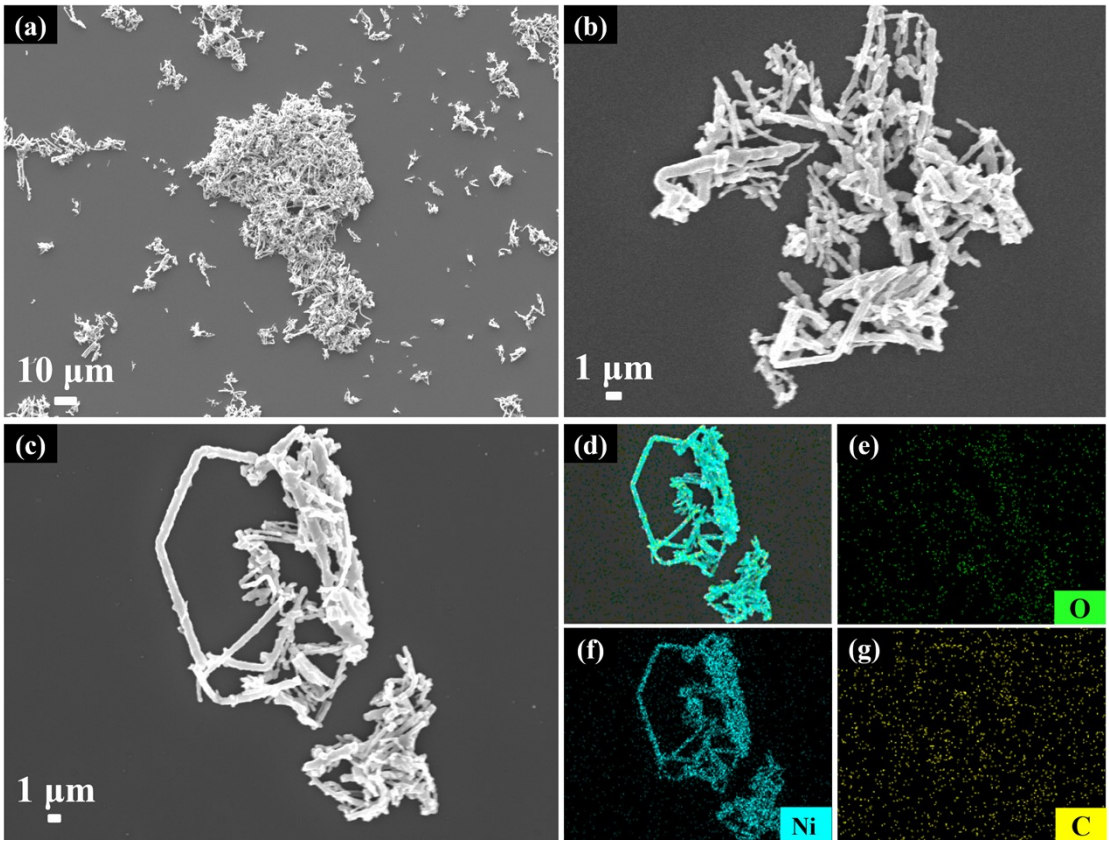


**Figure S3**. SEM image; (a-c) Ninw; (d-g) EDS characterization, where (e) is the O element;(f) is the Ni element; (g) is the C element.

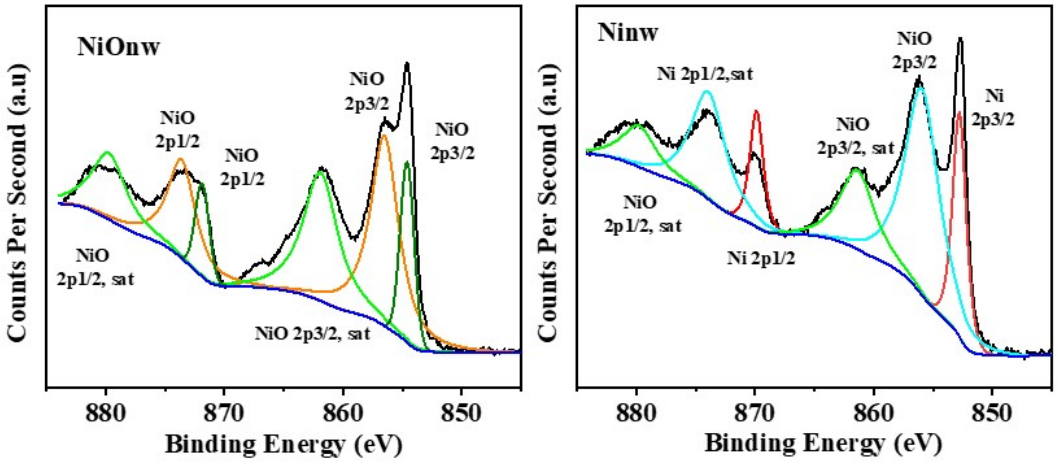


**Figure S4**. High-resolution XPS spectroscopy of Ni of (e) NiOnw (f) Ninw.

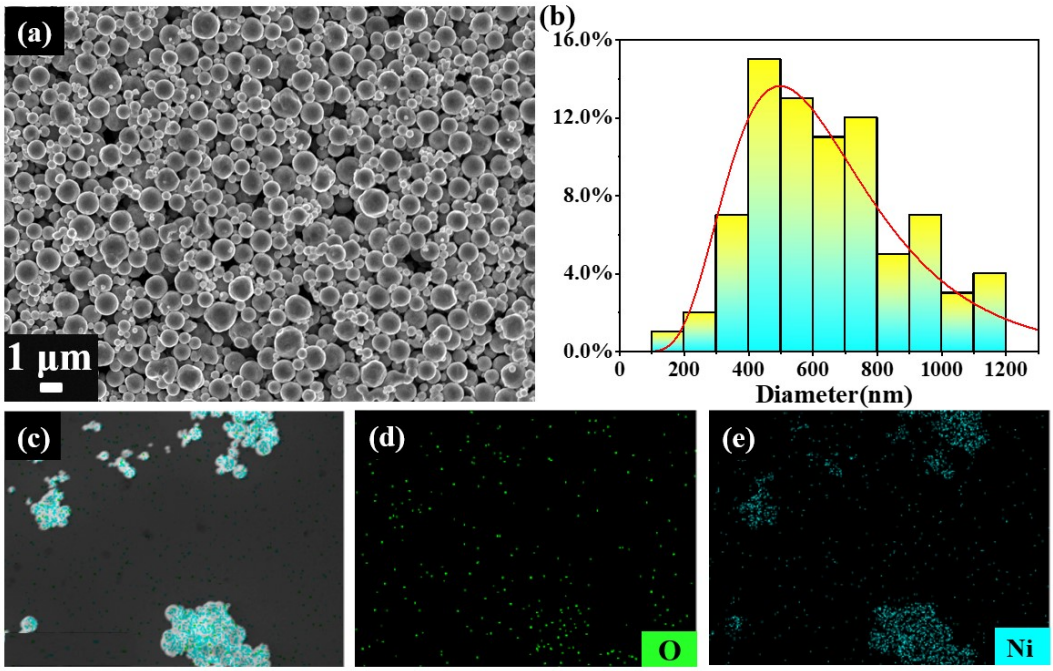


**Figure S5.** (a) SEM images of Ni powder; (b) grain size distribution map; (c-e) EDS characterization, where (d) is the O; (e) Ni

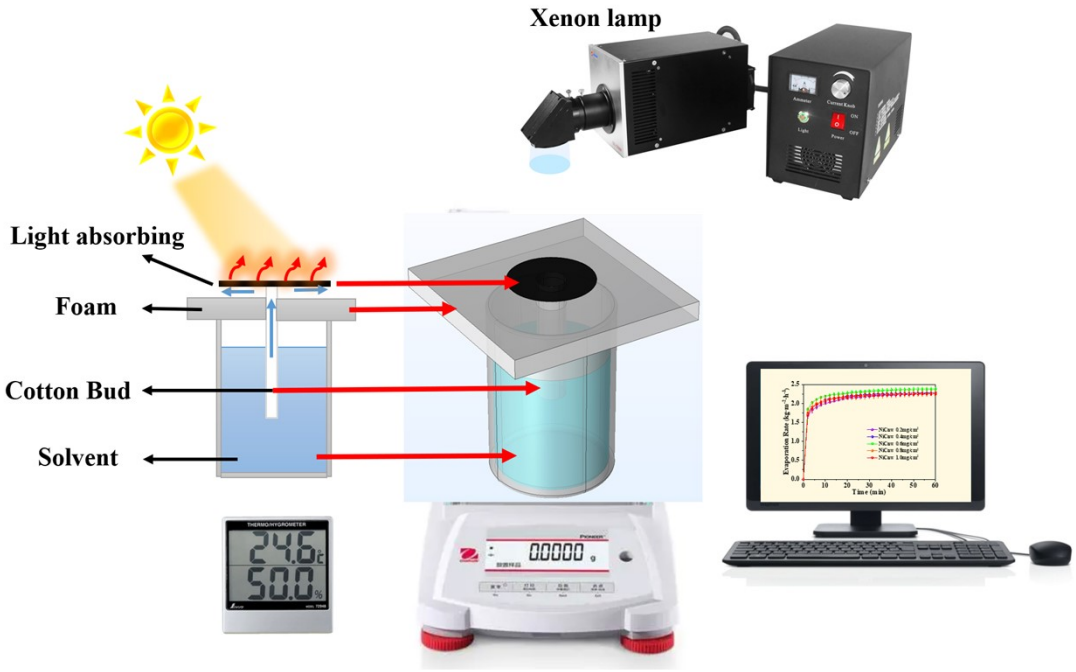


**Figure S6**. Schematic diagram of 1D interfacial evaporation system.

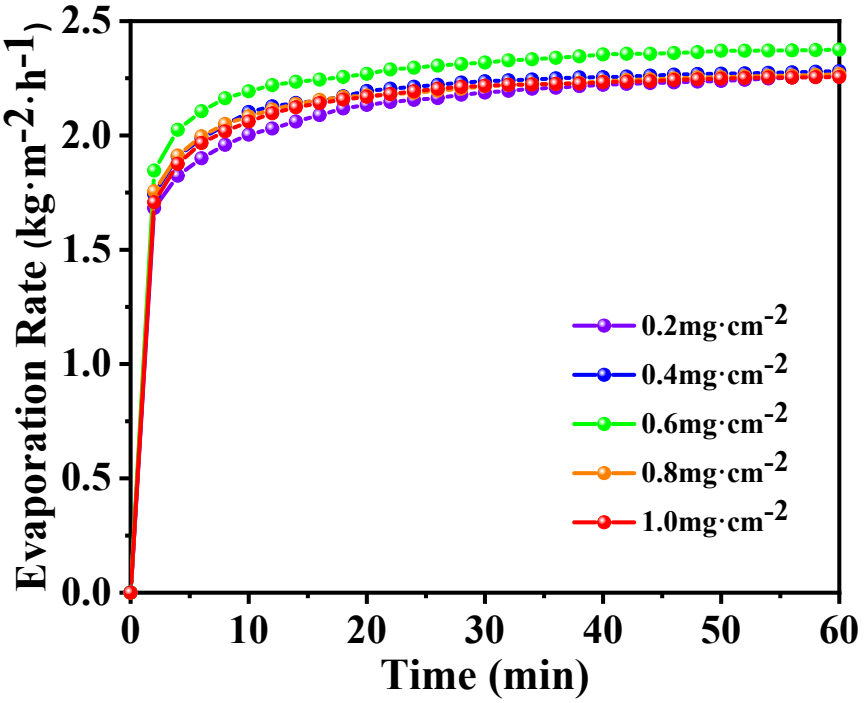


**Figure S7.** The evaporation rates of different surface loads of Ni@Cnw.

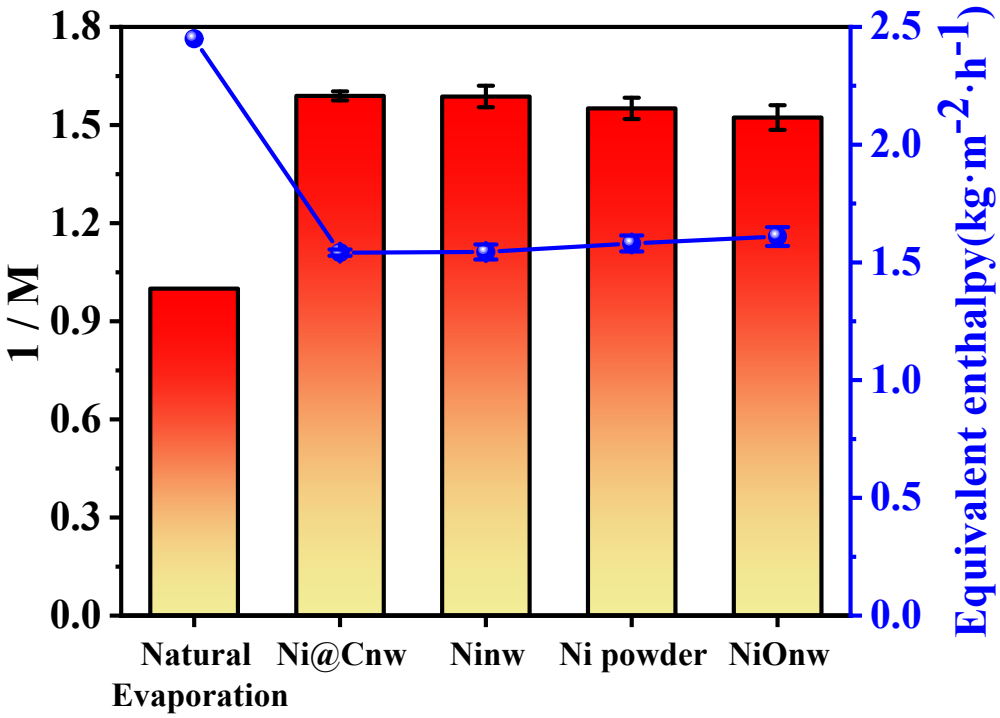


**Figure S8.** The ratio of evaporation rates of nickel-based nanowires photothermal conversion membranes in closed darkroom tests (1/M=photothermal conversion membranes: pure water) and equivalent enthalpy of evaporation

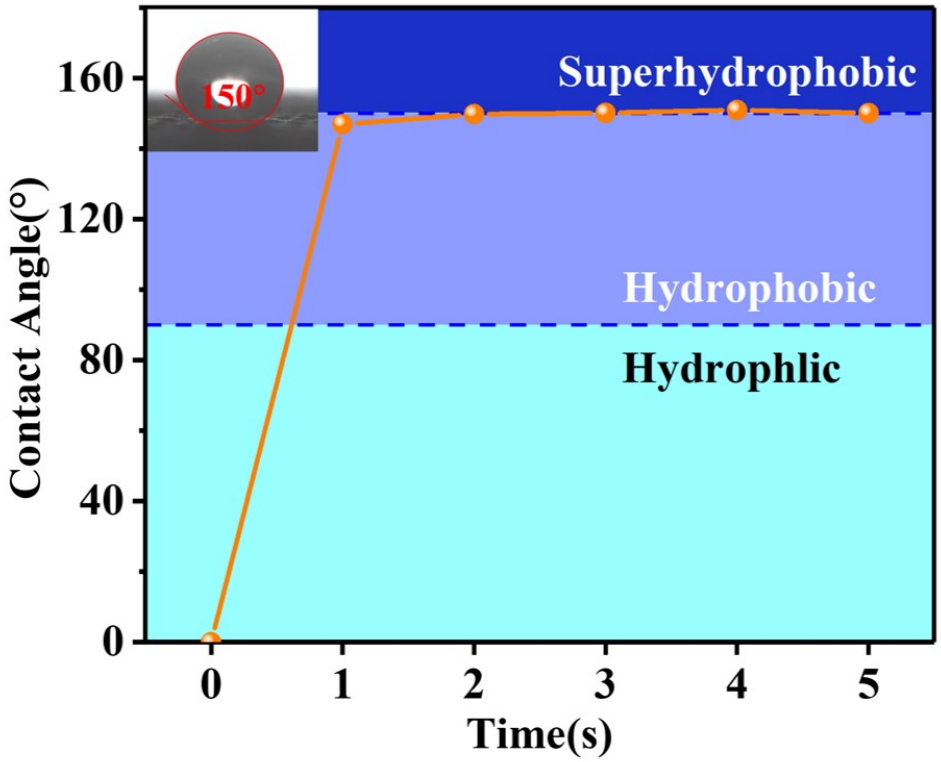


**Figure S9.** Contact angle test of PDMS modified SH-Ni@Cnw membrane with different spraying times.

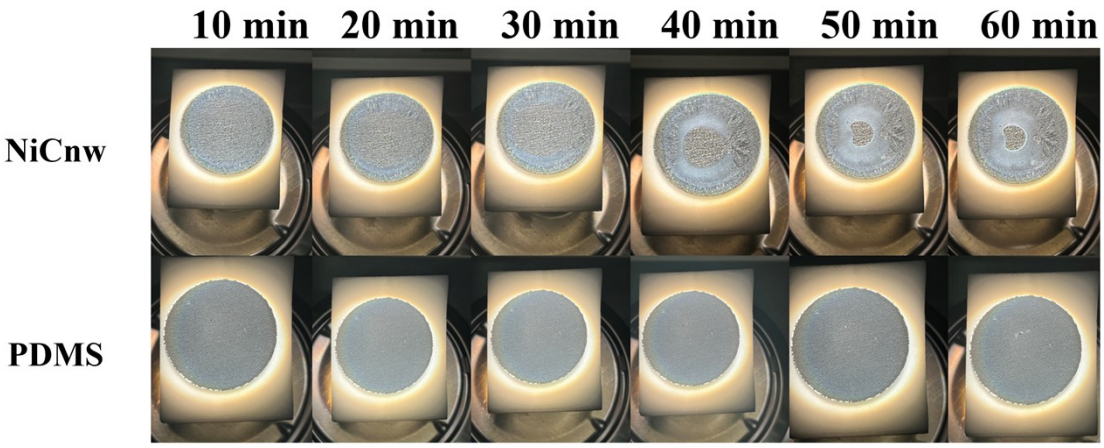


**Figure S10**. Salt precipitation on the surface of Ni@Cnw and SH-Ni@Cnw photothermal conversion membranes during the evaporation of seawater.


**Figure S11**. Schematic diagram of 2D interfacial evaporation system.

**Table S1.** The solar-driven interfacial evaporation performance based on different reported plasmonic metal materials.

| **Metal-based photothermal material** | **Power density / kW·m$^{-2}$** | **Evaporation rate / kg·m$^{-2}$·h$^{-1}$** | **Photothermal conversion efficiency / %** | **Reference** |
|---|---|---|---|---|
| **Ni@Cnw membrane** | **1** | **2.38** | **96.27** | **This work** |
| Ag NPs on pinecone | 1 | 1.82 | 100 | [1] |
| Nanoporous black Ag film | 1 | 1.42 | 92.6 | [2] |
| Au@polypyrrole | 1 | 1.33 | 93.38 | [3] |
| Black Au NPs-deposited sponge | 10 | 12.74 | 90.3 | [4] |
| Nanoporous black Au film | 1 | 1.51 | 94.5 | [5] |

## Reference


[1] Niazi, Z., Shafaee, M., Asarnia, M. and Goharshadi, E. K., *Korean Journal of Chemical Engineering*, 2024, 41(3), 807-817.

[2] Yu, B., Wang, Y., Zhang, Y., and Zhang, Z., *Nano Research*, 2023, 16, 5610-5618.

[3] Sun, Z., Huang, F., Cai, Y., Liang, W., Fan, S., Tu, C. and Liu, Y., Chemical Engineering Journal, 2024, 492, 152309.

[4] Y. Liu, Z. Liu, H. Huang, X. Liang, X. Zhou, H. Fu, Q. Wu, J. Zhang, W. Xie, Journal of Materials Chemistry A, 2019, 7(6), 2581-2588.

[5] Y. Zhang, Y. Wang, B. Yu, Z. Zhang, Advanced Materials, 2022, 34(21), 2200108.